Journal of Nano- and Electronic Physics
Vol. **10** No 3, 03027(8pp) (2018)

Журнал нано- та електронної фізики
Том **10** № 3, 03027(8cc) (2018)

Nanostructured ZnO Arrays Fabricated via Pulsed Electrodeposition and Coated with Ag Nanoparticles for Ultraviolet Photosensors

N.P. Klochko[1], K.S. Klepikova[1,*], S.I. Petrushenko[2], V.R. Kopach[1], G.S. Khrypunov[1], V.E. Korsun[1], V.M. Lyubov[1], M.V. Kirichenko[1], S.V. Dukarov[2], A.L. Khrypunova[1]

[1] *National Technical University "Kharkiv Polytechnic Institute", 2, Kyrpychov Str., 61002 Kharkiv, Ukraine*
[2] *V.N. Karazin Kharkiv National University, 4, Svobody Square, 61022 Kharkiv, Ukraine*

(Received 11 May 2018; published online 25 June 2018)

Nanostructured one-dimensional (1-D) ZnO arrays fabricated via pulsed electrodeposition and coated with Ag nanoparticles are researched with the aim of their using in the ultraviolet (UV) photosensors. The results of the crystal structure investigations showed that the pulsed electrodeposited zinc oxide arrays are polycrystalline in nature and matching with hexagonal wurtzite modification of ZnO. To enhance its UV photosensitivity, the silver nanoparticles (AgNPs) with different shape and an average size of 60 nm, as well as 300-500 nm long Ag nanorods with ~30 nm diameter, are precipitated mainly on the (002), (101) and (100) ZnO planes. Study of electrical properties and electronic parameters of the 1-D ZnO and Ag/ZnO nanocomposites using a current-voltage and capacity-voltage characteristics identified the important role of the high double Schottky barriers at the ZnO intergrain boundaries for the creation of great UV photosensitivity. It is proved that through monitoring the amount of AgNPs on the ZnO surface the electrical properties and electronic parameters of the Ag/ZnO nanocomposites, and consequently, the output parameters of the UV photosensors can be controlled.

Keywords: Ag/ZnO, Pulse electrodeposition, Capacitance-voltage characteristic, Ultraviolet photosensor, Structure, Electronic parameter.

DOI: 10.21272/jnep.10(3).03027 PACS numbers: 61.46.Km, 68.37.Ps

1. INTRODUCTION

Zinc oxide (ZnO) is a promising material for ultraviolet (UV) and visible (green) light optoelectronics, piezoelectronics, gas sensors, and dye-sensitized solar cells [1-7]. In particular, one-dimensional (1-D) ZnO nanostructured arrays are the most extensively used nanomaterials in the emerging fields of micro- and nanoelectronics owing to their excellent electrical, sensing, and optical properties. The specific feature of the various ZnO nanostructures with unique properties is the possibility of their synthesis by solution techniques such as electrodeposition, which not only appears as a low temperature alternative, but is also well suited for cheap large-scale production. According to [5], the pulsed electrodeposition ensures the best-controlled growth of ZnO nanostructured arrays with an antireflection effect and pronounced reversible hydrophobic-hydrophilic behavior, which can be managed by the ultraviolet irradiation. A combination of two promising nanomaterials, ZnO and silver (Ag), in fabricating of different Ag/ZnO heterostructure composites have been proposed recently in [5, 8-12] for the development of multifunctional nanosensors, including UV photosensors. In accordance with [5, 8, 13, 14], the most hopeful approach for the increasing the sensitivity of ZnO nanostructures is the creation of Ag/ZnO nanocomposites by the deposition of silver nanoparticles on the zinc oxide surface. Nevertheless, the mechanism of the ultraviolet photosensitivity of the Ag/ZnO nanocomposites is not fully understood. It was shown in [5, 8, 13-16], that illumination of Ag nanoparticles which are located on the ZnO surface leads to the occurrence of collective oscillations of conduction electrons inside the metal, i.e. plasmons. Under direct UV illumination these plasmon oscillations become resonant. This gives rise to a surface plasmon resonance (SPR). An interaction of Ag nanoparticles with ultraviolet radiation provides an intensive absorption of UV by the Ag/ZnO nanocomposites via the resonance of the free electron oscillations [16-17]:

$$\mathrm{Ag} + h\nu \rightarrow \mathrm{Ag}^*. \quad (1)$$

The photoinduced electrons generated from AgNPs due to SPR transfer from Ag to ZnO [16-17]:

$$\mathrm{Ag}^* + \mathrm{ZnO} \rightarrow \mathrm{Ag}^{\bullet +} + \mathrm{ZnO}(\bar{e}). \quad (2)$$

In addition, according to [16, 18], there are the Schottky barriers formed at the Ag–ZnO interface, thanks to which the separation of photogenerated electron–hole pairs is enhanced. These barriers efficiently impede the recombination of the photogenerated electron-hole pairs. Other authors [11, 19], on the contrary, observed the existence of the excellent ohmic contacts between Ag and ZnO without any Schottky barriers. At the same time, it is noted in [19] that the photosensitivity of Ag/ZnO samples with nanometer-sized materials is attributed to a band bending caused by built-in electric fields, that is, by potential barriers, which are considered as a favorable factor for the rapid transfer of photogenerated electrons. According to [20], the metal-semiconductor Schottky barriers on the ZnO surface determine the UV photosensitivity of single-crystal 1-D ZnO nanostructures. Apart from Ag/ZnO Schottky barriers, authors [20] consider a role of the oxygen in the

* catherinakle@gmail.com

creation of the surface potential barriers. In accordance with [20], in the dark the ZnO surface adsorbs oxygen molecules from the environment by providing free electrons [$O_2(g) + \bar{e} \rightarrow O_2^-(ad)$], therefore a depletion layer with low conductivity is formed near the surface. When exposed to UV light with photon energies higher than the band gap, electron–hole pairs are generated in ZnO [$h\underline{\nu} \rightarrow \bar{e} + h^+$]. The holes migrate to the surface and discharge the adsorbed oxygen ions [$h^+ + O_2^-(ad) \rightarrow O_2(g)$], causing desorption of the oxygen. Simultaneously, the unpaired electrons provide increased ZnO conductivity, which explains its UV photosensitivity. Similarly, authors [7] also describe the UV detection mechanism for single-crystal zinc oxide nanowires and silver-doped zinc oxide single-crystal nanowires exclusively through processes on the surface. Namely, due to adsorbed oxygen species (O_2^-, O_2^-, O^-), which are influenced by the near-surface and surface defects, that can act as charge carriers traps as well as adsorption sites. Similar to described in [7, 20] for single-crystal ZnO nanostructures, the above mechanism of the UV photosensitivity is commonly used [9, 15] for polycrystalline ZnO material, excluding an influence of the ZnO grain boundaries. However, the investigation of effect of the ZnO grain sizes on the UV sensitivity of the nanostructured ZnO arrays fabricated via pulsed electrodeposition and coated with Ag nanoparticles have approved unambiguously [5, 8] the existence of symmetrical double Schottky barriers φ, which occur in the ZnO grain boundary regions. The density of surface states N_{SS}, the concentration of uncompensated ionized donor impurity N_d and the width of the surface electron depletion region ω on both sides of the grain boundaries were calculated in [5, 8] using a current-voltage (*I-U*) and a capacity-voltage (*C-U*) characteristics. A correlation between above electronic parameters and UV sensitivity of the ZnO and Ag/ZnO nanostructures have been confirmed [5, 8]. Note, that the existence of the Schottky barriers in the ZnO grain boundary regions was not taken into account by the authors, who investigated UV sensors [9, 11, 20] or photocatalysts [12, 15-18] based on the nanocrystalline ZnO material. So, in this paper we present the results of studies that prove an important role of the symmetrical double Schottky barriers in the ZnO grain boundary regions in increasing of the photosensitivity of such objects. As examples, we use the 1-D ZnO nanostructure arrays electrodeposited in the pulsed mode and Ag/ZnO nanocomposites created on their base with Ag nanoparticles precipitated onto ZnO from silver sol. Here we show how it is possible to control the sensitivity of the ultraviolet photosensor via the amount of the AgNPs on the 1-D ZnO surface.

2. EXPERIMENTAL DETAILS

To fabricate nanostructured ZnO arrays the mode of pulsed electrochemical deposition was used in detail described in [21]. 1-D ZnO arrays with average length about 1.1 μm were obtained on the SnO_2:F/glass (or FTO) substrates using the potentiostatic stage of the ZnO seed layer formation during 30 sec and through the half-hourly pulsed electrodeposition, as shown in Fig. 1. For the creation of Ag/ZnO nanocomposites the colloidal solution of Ag nanoparticles (AgNPs) was prepared according to [22]. As it was previously described in [5, 8], the electrodeposited ZnO arrays were coated by AgNPs through their dipping into colloidal solution during 30 sec at 75 °C and subsequent drying in the air. After that, some of the Ag/ZnO nanocomposites were annealed in vacuum at 150 °C during 30 min. Similar to [5, 8] test samples Al/FTO/ZnO/Al and Al/FTO/(Ag/ZnO)/Al were fabricated by vacuum deposition of aluminum on limited areas (8.5 mm²) of FTO, ZnO and Ag/ZnO through a shadow mask and by applying a conductive adhesive with silver filler to the Al surface for a providing of galvanic contacts with copper microwires (Fig. 1).

The morphology of the zinc oxide arrays and Ag/ZnO nanocomposites was observed by scanning electron microscopy (SEM) in secondary electron mode. The SEM instrument (JEOL JSM-840) was operated at an accelerating voltage of 20 kV. Conductivity of the samples on the FTO substrates was sufficient for their study without the use of additional conductive coatings. Images of the Ag nanoparticles were obtained via transmission electron microscopy (TEM) using TEM instrument SELMI EM 125 at an accelerating voltage of 75 kV. For the TEM investigations, droplets of aqueous silver sol were dried on amorphous carbon films with the thickness of ~20 nm deposited on standard copper grids for electron microscopy. Amorphous carbon films were obtained by vacuum condensation on freshly cleaved single crystals NaCl at a residual gas pressure of 10^{-6} Torr created by an oil-free pumping system. After condensation, the crystals with the amorphous carbon films were extracted from the vacuum chamber and dissolved in distilled water, and then the films were caught on electron microscopy grids.

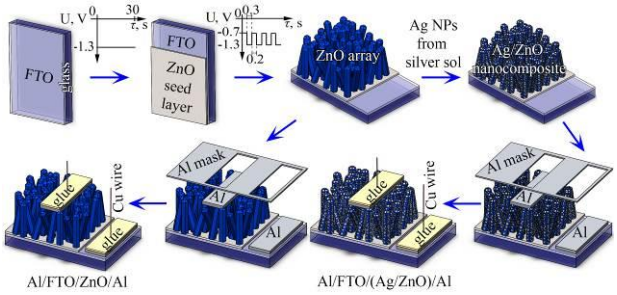

Fig. 1 – Schematic illustration of the ZnO array electrodeposition, Ag/ZnO nanocomposite creation, Al/FTO/ZnO/Al and Al/FTO/(Ag/ZnO)/Al test samples fabrications. The FTO potential – 1.3 V (relative to the silver/silver chloride reference electrode) used both for the potentiostatic ZnO seed layer deposition and as impulse potential during ZnO pulsed electrodeposition. Impulse duration is 0.2 sec. The FTO potential – 0.7 V used as the pause potential during ZnO pulsed electrodeposition, the pause duration is 0.3 sec

According to [23] the crystal structure of ZnO and Ag/ZnO was analyzed by using of X-ray diffraction patterns (XRD) recorded with "DRON-4" diffractometer in CoKα radiation using Bragg–Brentano focusing. The crystalline phases were revealed by comparing the recorded diffraction patterns and the reference JCPDS database. The crystal lattice constants a and c of the hexagonal zinc oxide were calculated from the positions

of the indexed lines in the X-ray diffraction patterns by the Nelson–Reilly graphical extrapolation method and refined using the least-squares method (LSM) by "UnitCell" software on the basis of all recorded reflections in the X-ray diffraction patterns, in accordance with [23]. The residual stresses in the ZnO arrays were calculated from the lattice constants of the electrodeposited and reference samples by using the elasticity constants of the material in various directions. In accordance with [23] the sizes of the coherent-scattering domains (D) of ZnO and microstrains $\Delta d/d$ were estimated using the Williamson–Hall approximation method. Similar to that described in [24] for the electrodeposited layers, it was suggested that D is equal to the average size of nanocrystalline ZnO grains.

Texture quality of the ZnO arrays was estimated by the method of Harris [1, 25]. Pole density P_i, which determines an axis of the crystal plane that is oriented normal to the surface was calculated according to the equation [1]:

$$P_i = N \cdot \left(I_i / I_{0i}\right) / \sum_1^N I_i / I_{0i}, \quad (3)$$

where I_i, I_{0i} are integral intensity of the i-th diffraction peak of the film samples and etalon, respectively; N is the number of lines presented in the diffraction. Texture axis has the index, which corresponds to the largest value of P_i. The orientation factor f for the relevant direction was calculated from the formula:

$$f = \sqrt{1/N \cdot \sum_{i=1}^{N} (P_i - 1)^2}. \quad (4)$$

Light and dark current-voltage characteristics, capacitance-voltage characteristics and temporal response curves under the influence of UV light were measured by using Al/FTO/ZnO/Al and Al/FTO/(Ag/ZnO)/Al test samples, as described in [5,8]. The light I-U characteristics of 1-D ZnO arrays and Ag/ZnO nanocomposites we measured under UV irradiation (wavelength was 365 nm) by using ultraviolet LED (LITEON (3 W)). Intensity (power density) of the light on the surface of the Al/FTO/ZnO/Al and Al/FTO/(Ag/ZnO)/Al test samples was 0.05 W/cm^2; 0.2 W/cm^2; 0.3 W/cm^2 or 0.5 W/cm^2. In accordance with [26] photosensitivity S of 1-D ZnO arrays and Ag/ZnO nanocomposites was calculated as ratio of the photocurrent I_p under UV to dark current I_d, which were measured at 1 V. To confirm stable work of test samples multiple "on– off" switching of UV irradiation was used. Similar to [5, 8], the measurement of C-U characteristics of 1-D ZnO arrays and Ag/ZnO nanocomposites was performed using a "Measurer L, C, R digital E7-12" at a frequency of 1 MHz and an amplitude of the measurement voltage 0.03 V. The measured C-U characteristics were analyzed as was proposed in [27] and used in [5,8,28-29].

3. RESULTS AND DISCUSSIONS

Fig. 2(a), (b), (c) presents top view SEM images of the 1-D ZnO nanostructured arrays fabricated via pulsed electrodeposition. Overview SEM image in Fig. 2(a) shows, that ZnO array is uniform and completely covers the FTO surface.

As seen in Fig. 2(b), this array consists of zinc oxide nanorods, which are located mainly perpendicular to the surface of the substrate, while, at the same time, they are partially disoriented in the same way as we showed early in [5, 8]. SEM image in Fig. 2(c) demonstrates "an erased blunt pencil"-type faceting of the zinc oxide nanorods with clearly visible (002), (101) and (100) faces. XRD pattern of ZnO array in Fig. 3(a) shows the prominent peaks corresponding to (002), (101) and (100) planes with greater intensity. Other peaks with low intensity were recognized as (102), (110), (103) and (112) planes of ZnO.

Thus, the pulsed electrodeposited array was polycrystalline in nature, matching with hexagonal wurtzite structure of ZnO (JCPDS 36-1451). As calculations of structural parameters have shown (Table 1), this ZnO array is preferentially oriented along the <001> direction. The coherent scattering domains D calculation via the Williamson–Hall have revealed, that the ZnO nanocrystal size D is in the range 40-50 nm. So, the D size never attained values corresponding to the ZnO nanorod length in Fig. 2.

As seen in the TEM image in Fig. 2(d), AgNPs have different shape and an average size of 60 nm. Some nanoparticles are 300-500 nm long Ag nanorods with ~ 30 nm diameter. Such a variety of forms of AgNPs is typical for silver nanoparticles precipitated from citrate sols without surfactants [30]. Top-view

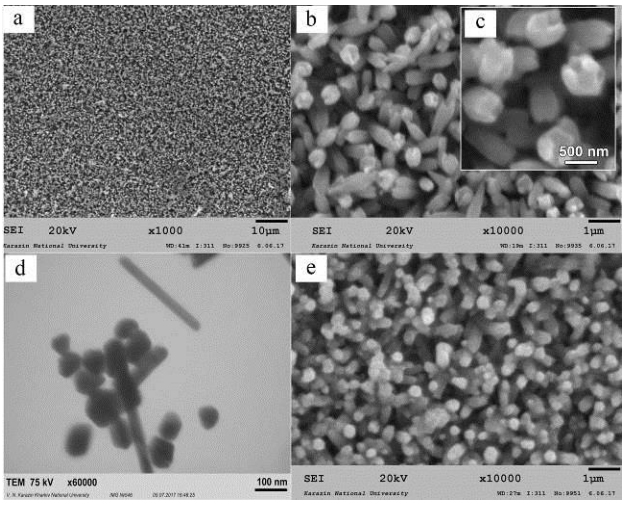

Fig. 2 – Top view SEM images of ZnO nanostructured arrays (a), (b), (c). TEM image of AgNPs (d). Top view SEM images of ZnO nanostructured array coated by Ag NPs (e)

SEM image of ZnO nanostructured array coated by AgNPs in Fig. 2(e) founds that they do not have a clear faceting, probably due to the silver nanoparticles are mainly adsorbed on the (002), (101) and (100) ZnO planes. The latter is confirmed by a change in the intensity of these zinc oxide peaks in the Ag/ZnO XRD patterns in Fig. 3(b), (c) as compared with Fig. 3(a), by a weakening of the ZnO preferential orientation along the <001> direction and by the orientation factor f decrease (Table 1). The presence of silver nanoparticles on the ZnO array surface is observed with the naked eye as brown-grey coloring, but the XRD patterns of

Ag/ZnO nanocomposites (see Fig. 3(b), (c)) do not contain peaks of silver or its compounds traces, both before and after vacuum annealing.

The significant ZnO crystal lattice strains and diffraction peak shifts that could be indicative of the formation of the solid solution $Zn_{1-x}Ag_xO$ were not observed. Similar XRD patterns we have shown for such objects earlier in [5, 8]. Note, that XRD patterns of the AgNPs layers deposited onto glass substrates via 30 cycles of their immersion in the silver sol, have been shown in [5, 8], represented (111) and (200) peaks characteristic of the cubic Ag modification (JCPDS 04-0783).

Fig. 4 displays *I–U* characteristics of the pulse electrodeposited 1-D ZnO array (Fig. 4(a)) and Ag/ZnO nanocomposite (Fig. 4(b)) in the dark and under *UV* radiation, which confirms the moderate photosensitivity of ZnO ($S \approx 4.2$ arb. units). Insert in Fig. 4(a) demonstrates photoresponse and recovery curves of the Al/FTO/ZnO/Al test sample at 1.0 V bias under "on-off" UV switching at different specific illumination powers from 0.05 W/cm² up to 0.5 W/cm².

Much greater sensitivity to the ultraviolet radiation is presented for Ag/ZnO nanocomposite (10 Ag NPs deposition cycles) in Fig. 4(b) ($S \approx 147$ arb. units). The presented in Fig. 4 *I–U* characteristics are symmetric with respect to the polarity of the applied voltage *U*. At $0 \text{ V} \le |U| < 0.5$ V the branches of the *I–U* characteristics of the ZnO array with $D \approx 40$-50 nm (Fig. 4(a)) are ohmic, while at $|U| > 0.5$ V they are superlinear, that qualitatively typical for the polycrystalline zinc oxide films and bulk varistors with ohmic metal contacts and double Schottky barriers at the intergrain boundaries [2]. The *I–U* characteristic of Ag/ZnO nanocomposite with 1-D ZnO array characterized by the about the same average size of nanocrystalline ZnO grains ($D \approx 30$-60 nm) covered with AgNPs (10 cycles) has very low current density in the dark (Fig. 4(b)). The probable reason is the formation of the Schottky barriers at the Ag/ZnO interfaces. Under *UV* illumination, the Al/FTO/(Ag/ZnO)/Al test sample with ZnO nanorods covered by AgNPs via 10 cycles of their treatment in the silver sol shows the largest increase in the current. So, as Fig. 4 and Fig. 5 demonstrate, the sensitivity of this Ag/ZnO nanocomposite to UV radiation is 35 times higher than that of the 1-D ZnO, which, according to [5, 8, 13-16], is the result of the surface plasmon resonance.

However, Fig. 5 shows also, that as the number of cycles of the AgNPs application exceeds 10, that is, as the amount of Ag NPs on the surface of 1-D ZnO increases, the photosensitivity decreases to $S \approx 3.8$ arb. units and even less. Furthermore, Fig. 5(b) demonstrates that the dark current on the semilog *I-U* characteristics increases, if the number of AgNPs cycles surpasses 10. To clarify the cause of the observed phenomenon we investigated electrical properties and electronic parameters of the 1-D ZnO and Ag/ZnO nanocomposites using their capacitance-voltage characteristics. The results of the measurements and calculations of *C-U* characteristics for 1-D ZnO arrays and

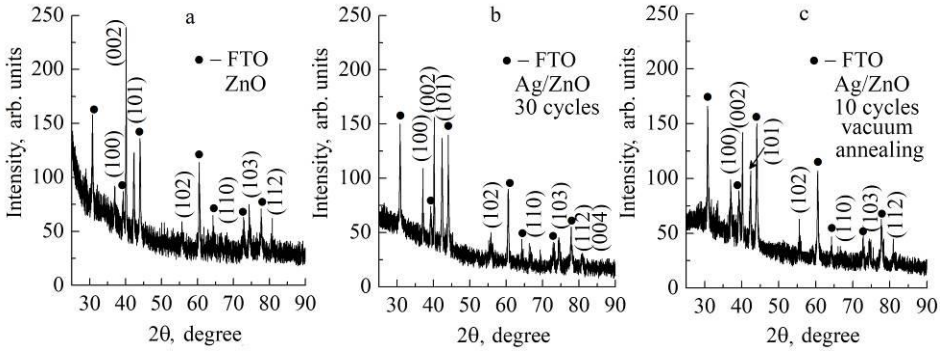

Fig. 3 – XRD patterns of nanostructured ZnO arrays electrodeposited in the pulsed mode (a) and Ag/ZnO nanocomposites fabricated by the deposition of AgNPs onto the ZnO surface for 30 cycles of processing in silver sol (b) and 10 cycles of processing in silver sol with subsequent vacuum annealing at 150 °C (c)

Table 1 – Structural parameters of the pulse electrodeposited ZnO and Ag/ZnO composites

Sample	Sizes of the coherent-scattering domains *D*, nm	Mcro-strains $\Delta d/d \times 10^{-3}$	Residual stresses, GPa	Lattice parameters, Å				Texture		
				Nelson–Reilly method		LSM		P_{hkil}	*hkl*	Orientation factor *f*
				a	*c*	*a*	*c*			
ZnO	40-50	0.3-1.4	– 0.49	3.256	5.215	3.255	5.217	2.1 1.3	(002) (102)	0.6
Ag/ZnO (AgNPs 10 cycles) vacuum annealing	30-60	1.1-2.4	– 0.40	3.267	5.211	3.251	5.215	1.5 1.2 1.1	(002) (103) (102)	0.3
Ag/ZnO (AgNPs 30 cycles)	30-60	1.6-2.5	-0.27	3.254	5.213	3.254	5.212	1.4 1.9	(002) (112)	0.4

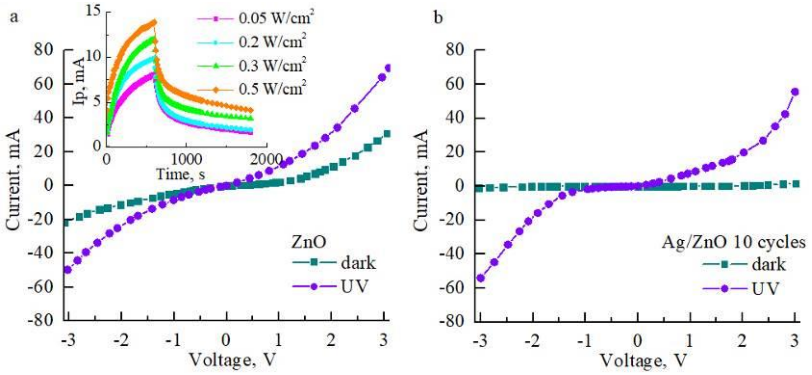

Fig. 4 – *I–U* characteristics of the test samples Al/FTO/ZnO/Al (a) and Al/FTO/(Ag/ZnO)/Al (b) in the dark and under UV radiation (UV wavelength is 365 nm; the specific UV illumination power is 0.5 W/cm²). Insert in (a) displays photoresponse and recovery curves of the Al/FTO/ZnO/Al test sample at 1.0 V bias under "on-off" UV switching (wavelength is 365 nm; the specific illumination powers are 0.05 W/cm²; 0.2 W/cm²; 0.3 W/cm² or 0.5 W/cm²)

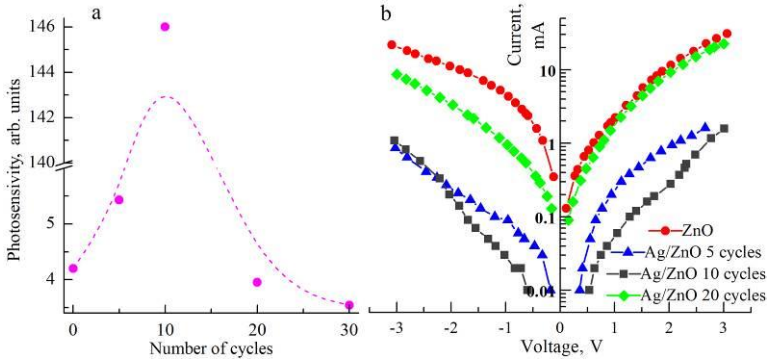

Fig. 5 – Photosensivity of 1-D ZnO array and some Ag/ZnO nanocomposites (a) at 1.0 V bias under UV (UV wavelength is 365 nm; specific UV illumination power is 0.5 W/cm²) and semilog dark *I–U* characteristics of the Al/FTO/ZnO/Al and Al/FTO/(Ag/ZnO)/Al test samples (b) depending on the number of the treatment cycles in the silver sol

Table 2 – Electronic and electrical parameters of 1-D ZnO array and Ag/ZnO nanocomposites

Sample	Sizes of ZnO coherent scattering domains D, nm	Number of Ag NPs deposition cycles	Concentration of uncompensated ionized donor impurity N_d, cm^{-3}	Surface state density N_{SS}, cm^{-2}	Barrier height φ, eV	Depletion region width ω, nm
ZnO	40-50	0	1.0×10^{16}	1.0×10^{11}	0.11	102
Ag/ZnO	30-60	10	6.7×10^{17}	1.6×10^{12}	0.42	24
Ag/ZnO	30-60	20	2.8×10^{14}	2.0×10^{10}	0.15	709

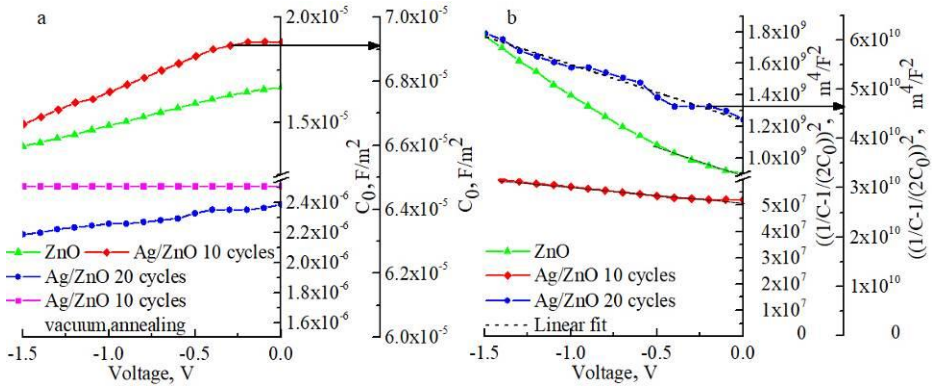

Fig. 6 – Bias-voltage dependences for the specific capacitances of the nanostructured ZnO arrays electrodeposited in the pulsed mode and Ag/ZnO nanocomposites based on them for the different number of AgNPs cycles before and after vacuum annealing (a). Graphs to define electronic parameters of ZnO and Ag/ZnO with the use of their *C-U* characteristics (b)

Ag/ZnO nanocomposites based thereon performed using the Al/FTO/ZnO/Al and Al/FTO/(Ag/ZnO)/Al test samples, correspondingly, are presented in Fig. 6 and in Table 2. It can be seen, that in the ZnO array having coherent scattering domains in the range 40-50 nm, the widths ω of the depletion regions caused by the intergrain Schottky barriers exceed size *D*; therefore, the barriers are not high ($\varphi \approx 0.11$ eV).

The value of concentration of uncompensated ionized donor impurity $N_d \approx 10^{16}$ cm^{-3} is typical [6] for nominally undoped n-ZnO due to shallow donor defects, namely, the oxygen vacancies and interstitial zinc. Both 1-D ZnO array and Ag/ZnO nanocomposites have high surface densities N_{SS} (from 2.0×10^{10} cm^{-2} to 1.6×10^{12} cm^{-2}), which confirms significant disorientation of the coherent-scattering domains.

Fig. 7 demonstrates schematically the creation of the intergrain Schottky barriers in the fabricated via pulsed electrodeposition ZnO nanorod and ZnO nanorods coated with Ag nanoparticles. Silver nanoparticles on the 1-D ZnO surface (10 Ag NPs deposition cycles) provide an increase in the height of the surface Schottky barriers (Fig. 7). The intergrain Schottky barriers have grown simultaneously ($\varphi \approx 0.42$ eV), since we observe the significant growth of the specific capacitance *C*. According to [8], such phenomena in polycrystalline semiconductors is due to the increasing of both the uncompensated ionized donor impurity concentration and the surface state density ($N_d \approx 6.7\times10^{17}$ cm^{-3} and $N_{SS} \approx 1.6\times10^{12}$ cm^{-2}, correspondingly, in Table 2). So far as only for some ZnO grains in the Ag/ZnO nanocomposite the depletion region width ($\omega \approx 24$ nm) does not reach half of the *D*, so, in the darkness there are very small regions, which contain high concentration of the uncompensated ionized donor impurity N_d inside the ZnO grains. That is, ZnO nanograins (or coherent-scattering domains *D*) are limited from all directions by the Schottky barriers. It is obvious that in this Ag/ZnO nanocomposite the depleted regions are formed not only near the ZnO surface due to the oxygen adsorption and because of the surface plasmon resonance via the AgNPs, but also along the boundaries of the ZnO coherent-scattering domains. As similar to the described in [20], obtained Ag/ZnO nanocomposites contain back-to-Schottky junctions on their surface and simultaneously they have intergrain Schottky barriers. The latter with barriers at the Ag/ZnO interfaces obstruct the transport of the charge carriers and contribute to the small dark current. Under UV irradiation, nonequilibrium charge carriers arisen in ZnO, and the photogenerated holes are directed by an electric field to the depletion regions in the intergrain Schottky barriers to reduce φ, as well as these photogenerated holes are used for the neutralization of the negative oxygen ion on the surface, ensuring the photodesorption of O_2 back to the environment.

Moreover, in accordance with [20], while the Ag/ZnO nanocomposite is under *UV* illumination, the increased charge carriers trapped at the Ag/ZnO interfaces lead to the reduction of the surface Schottky barrier height. As a result of the reducing of the above potential barriers and the increasing of the carriers (electrons) concentration under *UV* illumination, the electrical conductivity of the Ag/ZnO nanocomposite enhances greatly. In accordance with [4], when ZnO formation is carried out in an oxygen-containing medium, the acceptor levels on the grain boundaries, which create φ, are mainly native defects of interstitial oxygen O_i. To confirm the effect of the oxygen adsorbed on the ZnO surface and O_i defects in the intergrain boundaries on electrical properties and electronic parameters of Ag/ZnO nanocomposites, we researched Al/FTO/(Ag/ZnO)/Al test sample (10 AgNPs cycles) annealed in vacuum at 150 °C for 30 min to remove adsorbed O_2 and to decrease O_i concentration on the ZnO grain boundaries. As can be seen in Fig. 6, the vacuum annealed Ag/ZnO nanocomposite has low capacitance. Moreover, its *C* does not depend on voltage bias, therefore, it is completely in the flat band state, and namely, it is homogeneous insulator without any Schottky barriers.

If the number of AgNPs cycles exceeds 10, for example, as for the sample Ag/ZnO (20 AgNPs cycles) in Fig. 6, Fig. 7 and in Table 2, the silver nanoparticles cover adsorption centers on the zinc oxide surface significantly, not allowing for the oxygen to be adsorbed on it. As seen in *I–U* characteristics in Fig. 5 (b), the electrical conductivity along such Ag/ZnO nanocomposite

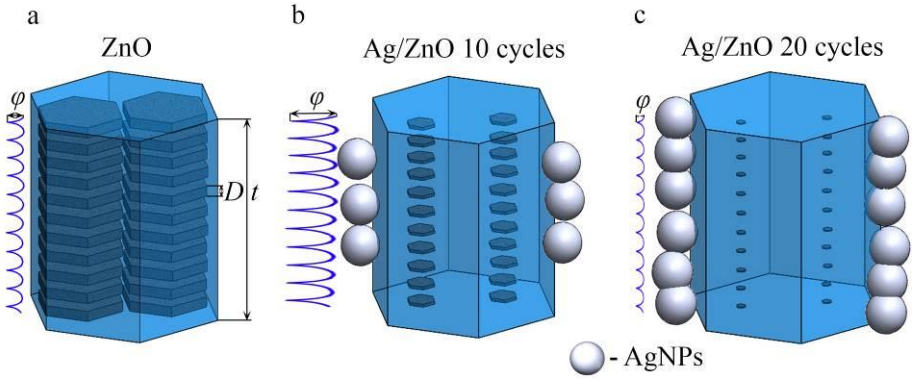

Fig. 7 – Illustration of the fabricated via pulsed electrodeposition ZnO nanorod and ZnO nanorods coated with Ag nanoparticles, depending on the number of the treatment cycles in the silver sol, in dark at exposure to ambient air. The dark blue hexagonal prisms correspond to the ZnO areas with large concentrations of charge carriers (electrons). The intergrain Schottky barriers φ, nanorod length *t* and coherent scattering domain size *D* are displayed

increases. The depletion region created by the Ag/ZnO Schottky barrier extends over the entire volume of the ZnO (depletion region width $\omega \approx 709$ nm). The ZnO grains are maximally depleted of charge carriers, they have low concentration of uncompensated ionized donor impurity ($N_d \approx 2.8\times10^{14}$ cm^{-3}) Surface state density on the grain boundaries is decreased ($N_{SS} \approx 2.0\times10^{10}$ cm^{-2}). Nevertheless, this material is not fully in the flat band state. As can be seen in Fig. 6, its capacitance is comparatively small, but depends on the voltage bias.

The results of the *C-U* measurements given in Table 2 confirm that the barriers at the boundaries of domains *D* in this sample are moderate ($\varphi \approx 0.15$ eV). Due to the low height of Schottky barriers, including near the surface of ZnO nanorods, Ag/ZnO nanocomposite with an excessive content of silver nanoparticles has weak UV photosensitivity ($S \approx 3.8$ arb. units in Fig. 5(a)). Its comparatively high conductivity, as can also be seen from its *I-U* characteristic in Fig. 5(b), may be because of the possible interconnection of the AgNPs deposited on ZnO, since the dimensions of the silver nanoparticles are commensurable with the regions of coherent scattering domains of zinc oxide.

4. CONCLUSIONS

The results of the investigations of the crystal structure presented in this work showed that the pulsed electrodeposited zinc oxide arrays, designed to create ultraviolet photosensor of a new generation, are nanocrystalline in nature and matching with hexagonal wurtzite modification of ZnO. Each individual ZnO nanorod is not a perfect single crystal, but it contains a certain number of coherent scattering domains, or nanograins, separated by their boundaries. To enhance its UV photosensitivity, the silver nanoparticles with different shape and an average size of 60 nm, as well as 300–500 nm long Ag nanorods with ~30 nm diameter, are precipitated mainly on the (002), (101) and (100) ZnO planes. The investigations of the electrical properties and electronic parameters of the 1-D ZnO and Ag/ZnO nanocomposites using the current-voltage and the capacity-voltage characteristics allowed us to determine the conditions for obtaining enhanced UV photosensitivity. The important role of the high double Schottky barriers created at the ZnO intergrain boundaries is identified for the Ag/ZnO nanocomposite having high sensitivity to the ultraviolet radiation. It is shown here, how by the controlling the amount of AgNPs on the ZnO surface it is possible to control the electrical properties and electronic parameters of the Ag/ZnO nanocomposites, and consequently, the output parameters of the UV photosensors of a new generation.

Conflicts of interests are not available.

Изготовленные импульсным электроосаждением и покрытые наночастицами Ag наноструктурированные массивы ZnO для ультрафиолетовых фотосенсоров

Н.П. Клочко[1], Е.С. Клепикова[1], С.И. Петрушенко[2], В.Р. Копач[1], Г.С. Хрипунов[1], В.Е. Корсун[1], В.Н. Любов[1], М.В. Кириченко[1], С.В. Дукаров[2], А.Л. Хрипунова[1]

[1] *Национальный технический университет «Харьковский политехнический институт», 2, ул. Кирпичева, 61002 Харьков, Украина*

[2] *Харьковский национальный университет им. В.Н. Каразина, 4, пл. Свободы, 61022 Харьков, Украина*

Исследованы наноструктурированные одномерные (1-D) массивы ZnO, изготовленные импульсным электроосаждением и покрытые наночастицами Ag, с целью использования их в ультрафиолетовых (УФ) фотосенсорах. Результаты исследования кристаллической структуры показали, что массивы оксида цинка, электроосажденные в импульсном режиме, поликристаллические и соответствуют ZnO гексагональной модификации вюрцит. Для увеличения УФ фоточувствительности были осаждены как серебряные наночастицы (AgНЧ) различной формы и размером в среднем 60 нм, так и нанострежни Ag длиной 300-500 нм и диаметром ~30 нм преимущественно на плоскостях ZnO (002), (101) и (100). Изучение электрических свойств и электронных параметров 1-D ZnO и нанокомпозитов Ag/ZnO с использованием вольт-амперных и вольт-фарадных характеристик позволило определить важную роль высоких двойных барьеров Шоттки на межзеренных границах ZnO для создания высокой УФ фоточувствительности. Доказано, что посредством регулирования количества AgНЧ на поверхности ZnO можно контролировать электрические свойства и электронные параметры нанокомпозитов Ag/ZnO и, соответственно, выходные параметры УФ фотосенсоров.

Ключевые слова: Ag/ZnO, Импульсное электроосаждение, Вольт-фарадная характеристика, Ультрафиолетовый фотосенсор, Структура, Электронный параметр.

Виготовлені імпульсним електроосадженням і вкриті наночастинками Ag наноструктуровані масиви ZnO для ультрафіолетових фотосенсорів

Н.П. Клочко[1], К.С. Клепікова[1], С.І. Петрушенко[2], В.Р. Копач[1], Г.С. Хрипунов[1], В.Є. Корсун[1], В.М. Любов[1], М.В. Кіріченко[1], С.В. Дукаров[2], А.Л. Хрипунова[1]

[1] *Національний технічний університет «Харківський політехнічний інститут», вул. Кирпичова, 2, 61002 Харків, Україна*

[2] *Харківський національний університет ім. В.Н. Каразіна, 4, пл. Свободи, 61022 Харків, Україна*

Досліджені наноструктуровані одновимірні (1-D) масиви ZnO, виготовлені імпульсним електроосадженням і вкриті наночастинками Ag, з метою їх використання в ультрафіолетових (УФ) фотосенсорах. Результати дослідження кристалічної структури показали, що масиви оксиду цинку, електроосадженні в імпульсному режимі, полікристалічні і відповідають ZnO гексагональної модифікації вюрцит. Для збільшення УФ фоточутливості були осаджені як срібні наночастинки (AgНЧ) різної форми і розміром в середньому 60 нм, так і наностржні Ag довжиною 300-500 нм і діаметром ~30 нм переважно на площинах ZnO (002), (101) та (100). Вивчення електричних властивостей і електронних параметрів (1-D) ZnO і нанокомпозитів Ag/ZnO, з використанням вольт-амперних і вольт-фарадних характеристик, дозволило визначити важливу роль високих подвійних бар'єрів Шоттки на міжзеренних межах ZnO для створення високої УФ фоточутливості. Доказано, що шляхом регулювання кількості AgНЧ на поверхні ZnO можна контролювати електричні властивості і електронні параметри нанокомпозитів Ag/ZnO і, відповідно, вихідні параметри УФ фотосенсорів.

Ключові слова: Ag/ZnO, Імпульсне електроосадження, Вольт-фарадна характеристика, Ультрафіолетовий фотосенсор, Структура, Електронний параметр.

REFERENCES

1. H.S. Sindhu, S. Joishy, B.V. Rajendra, A. Rao, M. Gaonkar, S.D. Kulkarni, P.D. Babu, *Mat. Sci. Semicon. Proc.* **68**, 97 (2017).
2. P.R. Bueno, J.A. Varela, E. Longo, *J. Eur. Ceram. Soc.* **28**, 505 (2008).
3. L.J. Brillson, W.T. Ruane, H. Gao, Y. Zhang, J. Luo, H. von Wenckstern, M. Grundmann, *Mat. Sci. Semicon. Proc.* **57**, 197 (2017).
4. H. Morkoç, Ü. Özgür, *Zinc Oxide: Fundamentals, Materials and Device Technology* (Weinheim: Wiley-VCH: 2009).
5. V.R. Kopach, K.S. Klepikova, N.P. Klochko, G.S. Khrypunov, V.E. Korsun, V.M. Lyubov, M.V. Kirichenko, A.V. Kopach, *Semiconductors* **51**, 335 (2017).
6. C.W. Litton, D.C. Reynolds, T.C. Collins. *Zinc Oxide Materials for Electronic and Optoelectronic Device Applications* (United Kingdom: John Wiley & Sons Ltd.: 2011).
7. O. Lupan, V. Cretu, V. Postica, M. Ahmadi, B.R. Cuenya, L. Chow, I. Tiginyanu, B. Viana, T. Pauporté, R. Adelung, *Sens. Actuat. B* **223**, 893 (2016).
8. V.R. Kopach, K.S. Klepikova, N.P. Klochko, I.I. Tyukhov, G.S. Khrypunov, V.E. Korsun, V.M. Lyubov, A.V. Kopach, R.V. Zaitsev, M.V. Kirichenko, *Sol. Energy* **136**, 23 (2016).
9. Y. Zhang, J. Xu, Q. Wang, Z. Pan, S. Ma, Q. Chen, *Mater. Res. Bull.* **73**, 119 (2016).
10. A.K. Pal, D.B. Mohan, *Appl. Surf. Sci.* **333**, 244 (2015).
11. Z. Yang, M. Wang, X. Song, G. Yan, Y. Ding, J. Bai, *J. Mater. Chem. C* **2**, 4312 (2014).
12. M. Hosseini-Sarvari, T. Ataee-Kachouei, F. Moeini, *Mater. Res. Bull.* **72**, 98 (2015).
13. Q. Simon, D. Barreca, D. Bekermann, A. Gasparotto, C. Maccato, E. Comini, V. Gombac, P. Fornasiero, O.I. Lebedev, S. Turner, A. Devi, R.A. Fischer, G. van Tendeloo, *Int. J. Hydrogen Energ.* **36**, 15527 (2011).
14. J.-C. Bian, F. Yang, Z. Li, J.-L. Zeng, X.-W. Zhang, Z.-D. Chen, J.Z.Y. Tan, R.-Q. Peng, H.-Y. He, J. Wang, *Appl. Surf. Sci.* **258** 8548 (2012).
15. Z. Han, L. Ren, Z. Cui, C. Chen, H. Pan, J. Chen., *Appl. Catal. B-Environ.* **126**, 298 (2012).
16. X. Zhang, J. Zhao, S. Wang, H. Dai, X. Sun, *Int. J. Hydrogen Energ.* **39**, 8238 (2014).
17. Y.I. Choi, H.J. Jung, W.G. Shin, Y. Sohn, *Appl. Surf. Sci.* **356**, 615 (2015).
18. H. Liu, Y. Hu, Z. Zhang, X. Liu, H. Jia, B. Xu, *Appl. Surf. Sci.* **355**, 644 (2015).
19. F. Yan, Y. Wang, J. Zhang, Z. Lin, J. Zheng, F. Huang, *Chem. Sus. Chem.* **7**, 101 (2014).
20. F. Yi, Y. Huang, Z. Zhang, Q. Zhang, Y. Zhang, *Opt. Mater.* **35** 1532 (2013).
21. N.P. Klochko, K.S. Klepikova, I.I. Tyukhov, Y.O. Myagchenko, E.E. Melnychuk, V.R. Kopach, G.S. Khrypunov, V.M. Lyubov, A.V. Kopach, *Sol. Energy* **120**, 330 (2015).
22. J. Bonsak, J. Mayandi, A. Thøgersen, E.S. Marstein, U. Mahalingam, *phys. status solidi c* **8**, 924 (2011).
23. N.P. Klochko, K.S. Klepikova, V.R. Kopach, G.S. Khrypunov, Y.O. Myagchenko, E.E. Melnychuk, V.M. Lyubov, A.V. Kopach, *Semiconductors* **50**, 352 (2016).
24. T. Ungár, G. Tichy, J. Gubicza, R. J. Hellmig, *Powder Diffr.* **20**, 366 (2005).
25. B.E. Warren. *X-ray Diffraction. Dover Books on Physics* (New York: 1990).
26. S. Dhara, P.K. Giri, *Rev. Nanosci. Nanotech.* **2**, 1 (2013).
27. K. Mukae, K. Tsuda, I. Nagasawa, *J. Appl. Phys.* **50**, 4475 (1979).
28. M.A. Ramírez, J.F. Fernández, J. Frutos, *Mater. Res.* **13**, 29 (2010).
29. I.V. Rozhanskii, D.A. Zakheim, *Semiconductors* 39, **577** (2005).
30. H. Xu, C. Kan, J. Wei, Y. Ni, C. Miao, C. Wang, S. Ke, D. Shi, *Plasmonics* **11**, 1645 (2016).